ELSEVIER

Contents lists available at ScienceDirect

Applied Surface Science

journal homepage: www.elsevier.com/locate/apsusc



Full Length Article



Investigation of (CrAlTiNbV) N_x high-entropy nitride coatings via tailoring nitrogen flow rate for anti-wear applications in aviation lubricant

Xiaolong Lu^{a,b,c}, Cunxiu Zhang^{a,d}, Cong Wang^{a,b}, Xinjian Cao^{a,b,c}, Rui Ma^{a,b,c}, Xudong Sui^{a,b,c,*}, Junying Hao^{a,b,c,*}, Weimin Liu^a

- a State Key Laboratory of Solid Lubrication, Lanzhou Institute of Chemical Physics, Chinese Academy of Science, Lanzhou 730000, China
- b Center of Materials Science and Optoelectronics Engineering, University of Chinese Academy of Sciences, Beijing 100049, China
- ^c Qingdao Center of Resource Chemistry and New Materials, Qingdao 266000, China
- ^d Department of Materials Science and Engineering, China University of Petroleum (East China), Qingdao 266580, China

ARTICLE INFO

ABSTRACT

Keywords: High-entropy nitride coatings Nitrogen flow rate Solid-liquid composite lubrication Aviation oil $(\text{CrAlTiNbV})N_x$ high-entropy nitride coatings are deposited via tuning nitrogen flow rates, and evaluating their influence on the microstructure, mechanical and tribological properties of the coatings. All deposited coatings exhibit columnar growth morphology and own a single face-center-cubic structure. As the nitrogen flow rate increases, the preferred orientation of the coating gradually transfers from (111) to (200) and (220), and then changes back to (111) with the nitrogen flow rate continues to increase. The S-38 sample possesses the optimal plastic deformation resistance and adhesion strength. Friction and wear results show that the $(\text{CrAlTiNbV})N_x$ coating deposited at nitrogen flow rate of 38 sccm owns the best tribological properties with a friction coefficient of 0.096 and wear rate of 1.8×10^{-7} mm³/(N·m) in 4050# aviation oil.

1. Introduction

As the rapid development of the modern aviation industry, the aviation transmission components will face higher speeds, loads and temperatures. How to extend the service life of moving parts such as bearings, hinges and gears is crucial to ensure the stable operation of aircraft. In today's perspective, protective coatings accompanied by a series of physio-mechanical advantages, including high toughness, good hardness, high corrosion resistance, as well as excellent adhesion to substrate, are playing an irreplaceable role in extending the service life of moving parts [1,2]. It has been discovered that hard coatings such as nitride and carbide of transition metals can effectively improve hardness and wear resistance, owing to the formation of mixed ion-metal-covalent bonds and nano-composite structure [3,4]. However, the traditional binary or ternary metal nitride and carbide coatings belong to the field of low-entropy films and cannot satisfy the growing demand. Lately, high-entropy alloys (HEAs) have become a hot spot for extensive research due to the advantages of superior structural properties. A multielement solid solution structure will be formed owing to the mixing entropy effect, which brings a series of advantages, including high strength, excellent anti-wear, and anti-oxidation. Recently, researchers

have introduced the concept of HEAs into coating preparation and proposed the concept of high-entropy films (HEFs) [5,6]. Due to the reduction of material dimensions and the addition of elements such as N or C, HEFs is even better than HEAs in certain properties [7-10]. For instance, Lai et al. [11] fabricated (AlCrTaTiZr)N coatings using magnetron sputtering and demonstrated that the mechanical properties were improved when compared to conventional transition metals nitride hard coatings. Several strengthening mechanisms of HEFs have been brought forward, including the phase composition, grain-size and solidsolution strengthening [12-14]. A series of factors in preparing the coating, including gas flow rates [15], sample bias [16,17], and deposition temperature [18], will greatly affect the structure and mechanical properties of the HEFs. For example, Liang et al. [19] fabricated (TiVCrZrHf)N coatings via tuning N2 flow rates and investigated their influences on the structure and mechanical properties of the coatings. Hsieh et al. [20] fabricated two non-equimolar high-entropy nitride coatings at different substrate biases, and the maximum hardness was reached 36.1 GPa and 36.7 GPa, which acquired at the bias of -100 Vand -150 V, respectively.

Therefore, in this article we will focus on the influence of N_2 flow rate on the microstructure and mechanical properties of (CrAlTiNbV) N_x

^{*} Corresponding author at: State Key Laboratory of Solid Lubrication, Lanzhou Institute of Chemical Physics, Chinese Academy of Science, Lanzhou 730000, China. E-mail addresses: suixudong@licp.cas.cn (X. Sui), jyhao@licp.cas.cn (J. Hao).

 Table 1

 Atomic radius of each element in multi-element (CrAlTiNbV) splicing target.

	Cr	Nb	Ti	Al	V
Atomic radius (Å)	1.4	1.45	1.4	1.25	1.35

Table 2Deposition parameters for the coatings.

Coatings	Ion cleaning	Cr binding layer	Top layer
Cr target power (DC, A)	0.4	4.5	0
CrAlTiNbV target power (DC, A)	0.4	0	4.5
Bias voltage (V)	-450	-60	-36
Ar flow rate (sccm)	18	18	18
N ₂ flow rate (sccm)	0	0	18/28/38/ 48
Deposition time (min)	30	8	233

high-entropy nitride coating. At the same time, considering that there are few studies on the solid–liquid composite lubrication of high-entropy coatings in the aviation lubricant environment, this article will study the tribological properties of the deposited high-entropy nitride coatings in aviation lubricant (4050#). The research in this paper hopes to supply theoretical support for the development of high-entropy nitride coatings in the future, and help to have a more detailed understanding of the solid–liquid composite lubrication required by advanced aircraft engines.

2. Experimental details

2.1. Coating deposition

(CrAlTiNbV)Nx coatings are fabricated by using magnetron sputtering method. The substrates are AISI 440C steels and Si (100) wafers. A multi-element splicing target (contains five elements of Cr, Al, Ti, Nb and V) is used for depositing the (CrAlTiNbV)N_x coatings. The atom sizes of these metal elements are listed in Table 1. The size difference of these atoms is conducive to the formation of a single FCC structure. Before deposition, all samples need to be ultrasonically cleaned in acetone and in ethanol for 20 min, respectively. Then they are blown dry by compressed air and quickly put into the vacuum chamber. During deposition, pure argon is introduced and the flow ratio maintains 18 sccm after the background pressure is pumped to 3.0×10^{-3} Pa. All the samples are Ar⁺-cleaned for 30 min to remove the surface oxides and contaminants. To improve the adhesion strength of the coating, a Cr interlayer between the coating and the substrate is deposited firstly. Various nitride coatings are deposited at an applied substrate bias of -36 V under different N₂ flow rates of 18 sccm, 28 sccm, 38 sccm, and 48 sccm, respectively. In order to facilitate the following discussion, the samples prepared under different N2 flow rates are named S-18, S-28, S-38 and S-48. The deposition details are summarized in Table 2.

2.2. Coating characterization

To observe the microstructure, a field emission scanning electron microscope (FESEM, JSM-7610F) is taken for acquiring cross-sectional images of the deposited coatings. In the same equipment, the energy dispersive spectroscopy (EDS, OXFORD) is used to evaluate the element compositions of the coatings. The crystalline structure of the deposited coatings is detected by X-ray diffractometer (XRD, D8 ADVANCE) using Cu K α radiation. The incident angle is chosen as 1°. The topography is measured by an atomic force microscope (AFM, NanoWizard 4). The hardness and modulus of the deposited coatings are tested by a nanoindentation technique (AGILENT, G200). The indentation depth is no more than 1/10 of the coating's thickness, which can neglect any

Table 3 Physicochemical properties of 4050# lubricating oil.

	lubricating oil	Kinematic viscosity (v/ mm ² ·s ⁻¹)		Acid value (mgKOH/g)	Flash point (/°C)	Pour point (/°C)
		40 °C	100 °C			
-	4050#	24.82	5.091	0.05	252	-57

substrate effect. Five indentations are measured to acquire the mean value and standard deviation. The adhesion behavior of the coatings to the substrate is studied by the scratch tester equipment (MFT-4000) with a diamond rockwell indenter HRC-3 of 120° cone angle and 0.2 mm tip radius, whereas a termination load of 100 N with the loading rate of 80 N/min is used in scratch tests. An optical microscope (OM, NMM-800TRF) is used to observe the scratch track surface.

2.3. Friction and wear test

The tribological tests are evaluated by a ball-on-disc tribometer (CSM). The tests are carried out in ambient air at RT and relative humidity of 40%. The AISI 440C steel ball with a diameter of 6 mm is chosen as the counterpart material. The friction radius is 2 mm and the sliding velocity is 6.28 cm/s. The applied load is 20 N and the calculated Hertz contact stress is 1.85 GPa. Aviation refined oil 4050# is bought from Sinopec Lubricant Co., Ltd. Table 3 exhibits the physicochemical properties of the aviation oil. After the tribological test, an optical microscope (OM, NMM-800TRF) is used to record the optical morphology of the wear track. The wear volume is determined by a portable surface roughness tester (Surftest SJ-210). The wear rate (w) of the coatings is determined by volume loss and according to the following formula:

$$w = V/NS \tag{1}$$

where V is the wear volume (mm³), N is the applied load (N) and S is the total sliding distance (m).

3. Results and discussion

3.1. Structure and morphology

Fig. 1 shows cross-sectional images of (CrAlTiNbV)N_x coatings deposited under different N_2 flow rates. The thickness is 0.93 μm , 0.8 μm, 0.8 μm and 1.13 μm for the coatings marked with S-18, S-28, S-38 and S-48, respectively, whereas the thickness of Cr binding layer for all samples is approximately 150 nm. The results reveal that all samples possess typical columnar microstructures. As the N₂ flow rate increases, the coating structure is getting more dense and compact, and the S-38 sample achieves the densest and finest columnar structure. This is because that the metal atoms sputtered from the multi-element splicing target can combine with N2, which can produce a single-phase solid solution structure. The formed nitride phase can dense the coating structure. When the N2 flow rate reaches 48 sccm, the formation of Ncontaining layer on the target surface can result in a decrease in the conductivity of the target and a decrease in the efficiency of argon-ion bombardment of the target, that is, the "target poisoning" phenomenon occurs. The combined metal atoms with N₂ are greatly reduced, and the large metal nitride particles sputtered directly from the surface of the poisoned target, which leads to an increase in the lateral size of columnar crystals of the coating.

Fig. 2 displays the composition of (CrAlTiNbV) N_x coatings as a function of N_2 flow rate. Accompanying the increase of N_2 flow rate, the N concentration increases and reaches over 40 at.% for the S-48 sample, which exhibits gradually saturated tendency. This is considered to be an under-stoichiometric nitride coating. The Cr concentration in the coating is relatively higher than that of other metal element owing to its

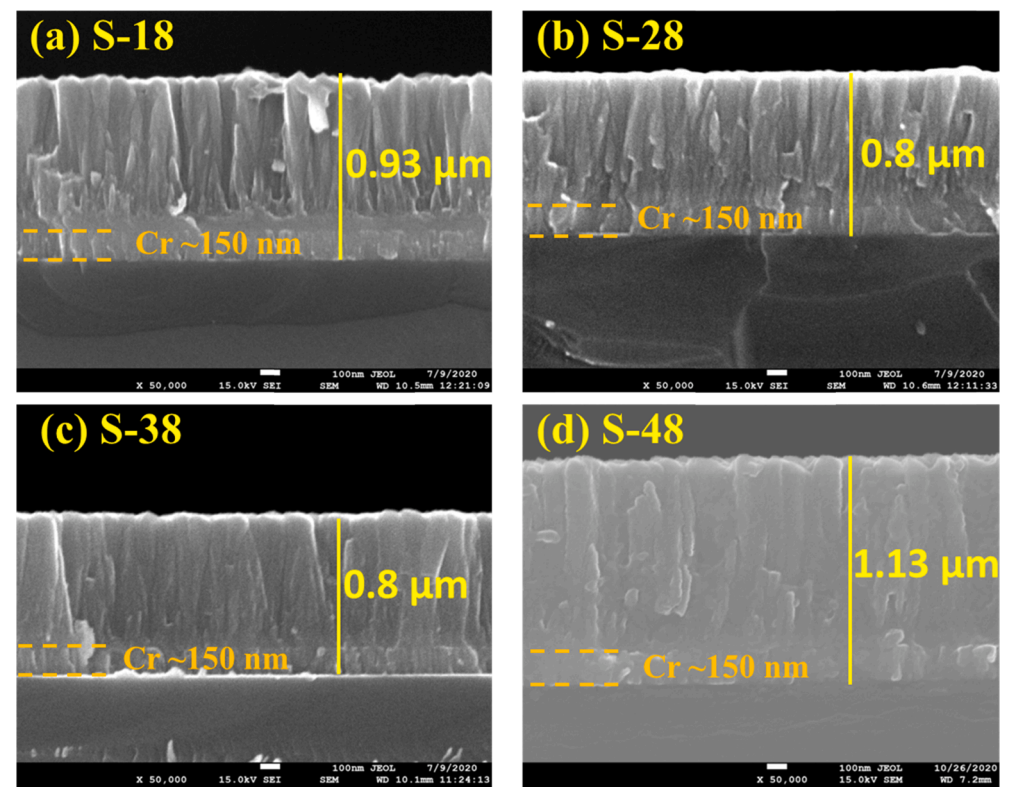


Fig. 1. SEM images of (CrAlTiNbV)N_x coatings deposited at different N₂ flow rates: (a) 18 sccm; (b) 28 sccm; (c) 38 sccm and (d) 48 sccm.

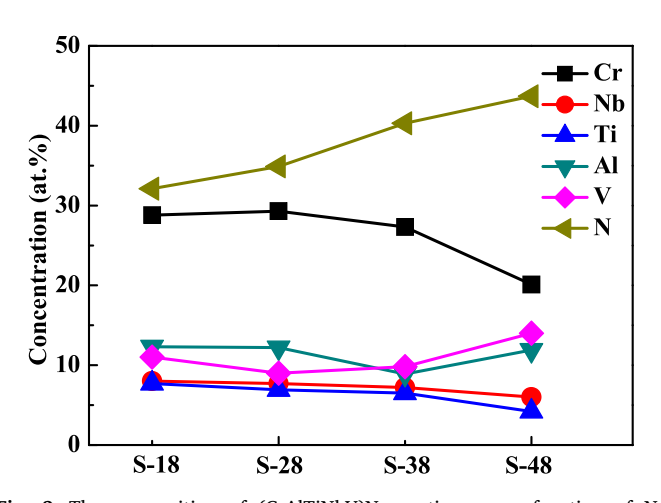


Fig. 2. The composition of $(\mbox{CrAlTiNbV})N_x$ coatings as a function of N_2 flow rate.

higher sputtering rates than that of other element in the splicing target. In addition, since the EDS analysis technology has a light spot with a diameter of about 1 μm , it will be affected by the Cr transition layer during the quantitative analysis of the cross-sectional SEM. Therefore, both effects can result in a higher Cr concentration measured in the coating.

Fig. 3 presents the XRD result of (CrAlTiNbV) N_x coatings deposited under various N_2 flow rates. It is displayed that (CrAlTiNbV) N_x coatings own a single FCC NaCl-type solid solution structure, indicating the formation of high-entropy nitride coating. This is similar to the results of previously reported coatings, such as (AlCrNbSiTiV) N_x (TiVCrZrHf) N_x and (AlMoNbSiTaTiVZr) N_x [21–23]. The result reveals that the single solid-solution phase can be formed and stabilized by multi-component nitrides due to high entropy effect. With the increase of N_2 flow rate

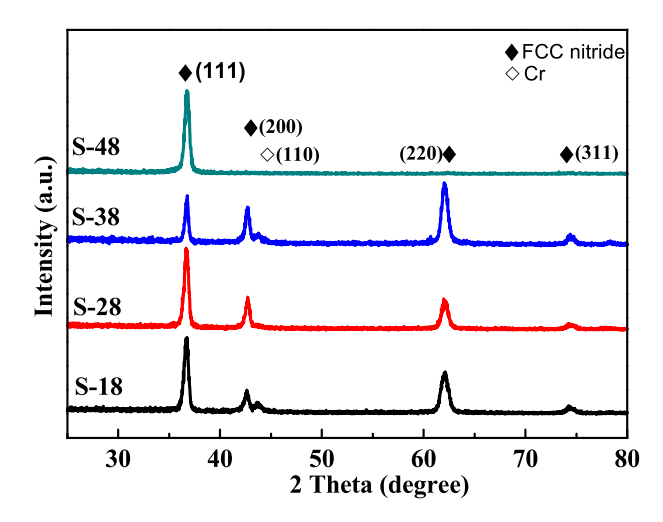


Fig. 3. XRD results of (CrAlTiNbV) $N_{\rm x}$ coatings deposited at different $N_{\rm 2}$ flow rates

from 18 sccm to 38 sccm, the preferred orientation of the coating structure is transformed from (111) to (200) and (220), and then changes back to (111) with the N_2 flow rate continues to increase. The transition of the preferred orientation of high-entropy nitrides can be explained by both thermodynamics and kinetics. From the point of thermodynamics view, the increment of N_2 flow rate can increase the mobility of atoms, which can promote the formation of a closed packed structure. To achieve a stable state, the (200) plane with the lowest surface energy is anticipated to be the preferred orientation under the conditions of thermodynamic equilibrium. It is pointed out that the (111) plane has the lowest strain energy, and is favored under high strain conditions [23]. Therefore, on the basis of the difference of accumulated strain in the coating, it can be used to explain the

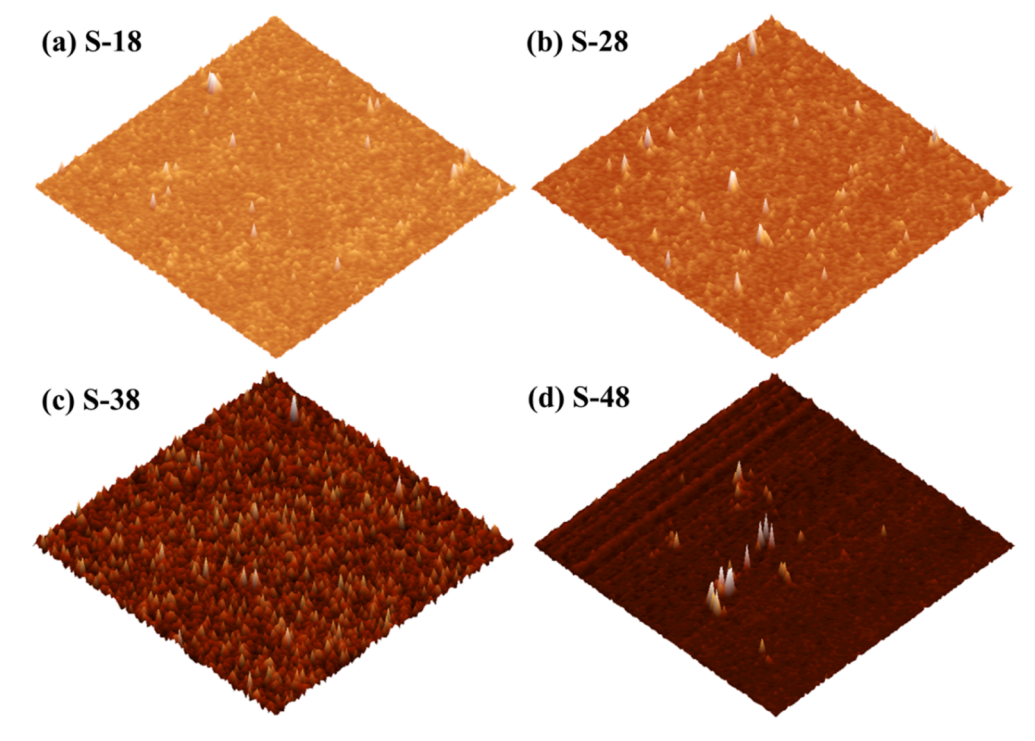


Fig. 4. Surface morphology of (CrAlTiNbV) N_x coatings deposited at different N_2 flow rates: (a) 18 sccm; (b) 28 sccm; (c) 38 sccm and (d) 48 sccm.

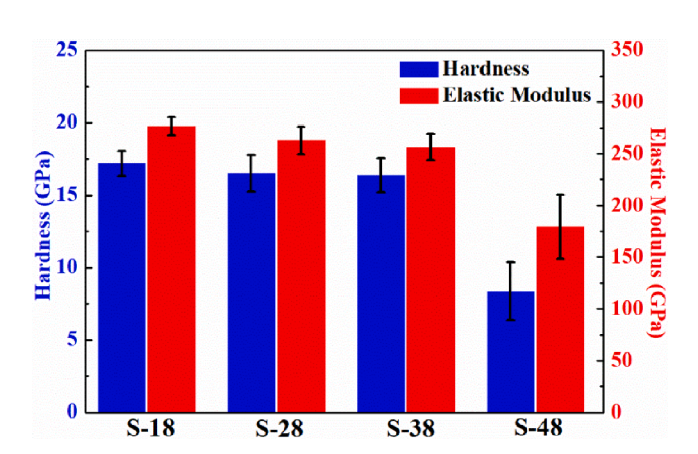


Fig. 5. Hardness and elastic modulus of (CrAlTiNbV) $\!N_x$ coatings as a function of N_2 flow rate.

transformation of the preferred orientation at higher N2 flow rate. As the N₂ flow rate increases, the average energy of particles bombarding the coating surface decreases, which leads to a decrease in coating strain. Therefore, the transition of the preferred orientation in coating from (111) to (200) and (220) is accompanied by a decrease in coating strain. The preferred orientation of the coating changes back to (111) with the N₂ flow rate increases to 48 sccm. The excessive N₂ flow weakens the mobility of atoms, and a large number of atoms per unit area gathering at (111) orientation with the lowest strain energy, thus, the (111) preferred orientation is formed at low energy sites. In view of kinetic reasons, the (111) orientation possesses the densest array direction, while the (200) and (220) represent for the most open channeling planes [17]. Therefore, coating texture evolves towards the (200) and (220) planes to obtain the highest probability of surviving as the mobility of atoms increases, while metal atoms are hard to diffuse on the (111) plane due to its kinetically limited growth [24].

Fig. 4 presents AFM surface morphology of (CrAlTiNbV) $N_{\rm x}$ coatings deposited under various N_2 flow rates. By observing the AFM images,

there are dome-shaped nanostructured particles in the (CrAlTiNbV) $N_{\rm X}$ coatings, which are related to the competitive growth of the coatings. As the N_2 flow rate increases, the surface atom diffusion and grain boundary motion are accelerating by a strong driving force. Under the conditions of thermodynamic equilibrium, the required surface and interface energy are expected to obtain the minimum energy in a way of forming the new islands [25]. Based on the XRD results shown in Fig. 3, the preferred orientation of the coating gradually transfers from (111) to (200) and (220) as the N_2 flow rate increases to 38 sccm. Namely, the surface and interface energy consideration favor the growth of (200) and (220) in this study. However, for the S-48 sample, the replacement of reactive sputtering of coatings with direct sputtering of nitride coatings results in the sputtering of large particles, which contributes to the formation of abnormally grown particles on the coating surface.

3.2. Mechanical and tribological properties

Fig. 5 presents the hardness and elastic modulus of (CrAlTiNbV)N_x coatings as a function of N2 flow rate. Generally, the hardness of the coatings is proportional to its wear resistance capability, which is highly affected by grain size, densification and residual stress. Accompanied by the increase of N2 flow rate, the hardness of the coatings exhibits a slightly downtrend. However, as the N2 flow rate continues to increase, the S-48 sample reaches the lowest hardness value (8.36 GPa). Several major reasons for this phenomenon are taken into consideration. Firstly, according to the Hall-Petch effect, the grain size can affect the hardness of the coatings. Coating structure with a smaller grain size indicates that there are more grain boundaries, which can better suppress dislocation slip. As displayed in the SEM images of Fig. 1, the columnar crystal size of the S-48 sample is larger than that of other samples, which results in a decreased hardness. Secondly, it is pointed out that the solid-solution strengthening effect caused by the introduction of different-size atoms can contribute to the coating hardening [11]. However, the excessive N concentration will result in the formation of nitride on the multi-element target surface (target poisoning phenomenon), which can replace the reactive sputtering of coatings with direct sputtering of nitride coatings, thereby reducing the hardness and elastic modulus of the coatings [26].

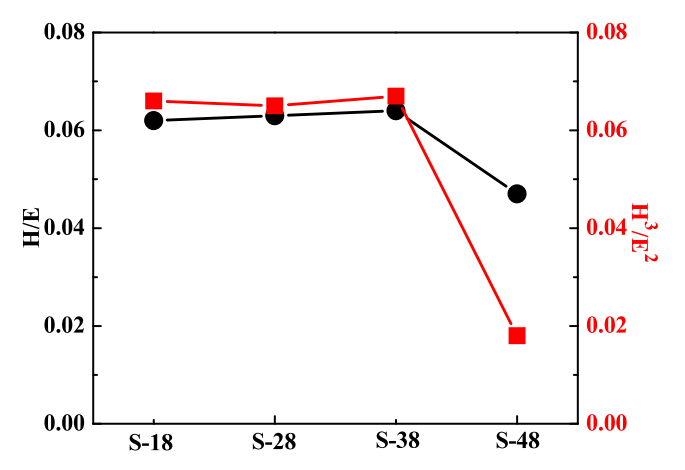


Fig. 6. H/E and ${\rm H^3/E^2}$ values of (CrAlTiNbV)N_x coatings as a function of N₂ flow rate

Thirdly, as the N_2 flow rate reaches 48 sccm, the formation of columnar structure growth defect, such as columnar coarse crystals and high void concentration, can result in a decrease in the hardness of the coatings. In general, the ratio of hardness to modulus (H/E) indicates the required elastic energy for fracture failure, which can reflect the wear resistance of the coating to some extent, and the H^3/E^2 value represents for the coating's resistance to plastic deformation [27]. Fig. 6 presents the values of H/E and H^3/E^2 as a function of N_2 flow rate. The H^3/E^2 value increases as the N_2 flow rate increases from 18 sccm to 38 sccm, which demonstrates that the plastic deformation resistance of the coating is improved. However, the decrease in the H/E and H^3/E^2 values for the S-48 sample indicates a degradation of plastic deformation resistance.

To evaluate the adhesion behavior of the coatings, scratch tests are performed on all samples. Plots of acoustic emission signal, friction force and friction coefficient as a function of the applied normal load are presented in Fig. 7. The corresponding scratch images are shown in Fig. 8. In this study, a lower critical load $L_{\rm Cl}$ is used to indicate the initial failure of coatings, which always associates with failure modes, such as

the first cracking inside the scratch track and the event of partial spallation at the track edge. LC1 belongs to the cohesive failure, and can be expressed as the fracture resistance behavior of the coating [28]. The combined analysis based on the sudden change in friction coefficient and the fluctuation of the acoustic signal in Fig. 7, as well as the scratch images in Fig. 8 is used as the criterion to determine the critical load LC1 of the coatings. As displayed in Fig. 7, a load of ~17.5 N for the S-18 sample is identified as L_{C1}, owing to the sudden increase in friction coefficient at a load of 17.5 N, as well as the appearance of a strong acoustic emission signal peak at this location. Similarly, the value of LC1 for the S-28 and S-38 sample is determined as \sim 16.5 N and \sim 32 N, respectively. However, the acoustic emission signal peak is disappeared for the S-48 sample, and remains stable with the forward movement of the indenter under the continuously increasing load. Accordingly, the L_{C1} value (~10 N) for the S-48 sample is determined by the combined analysis of the friction coefficient curve in Fig. 7 and the scratch images in Fig. 8. So, the adhesion strength of the coatings first improves with the increment of N2 flow rate, and the optimal value is obtained at the S-38 sample, and then decreases with the N2 flow rate continues to increase.

For all samples, the transverse cracks inside the scratch and spallation along the scratch are shown in Fig. 8, however, within the tested load range, the indenter does not completely through the coating. So, a higher critical load L_{C2}, indicating the complete adhesion failure between the coating and the substrate, is not appear in this study. There exist a lot of arc-shaped transverse cracks inside the scratch and spallation along the scratch track sides for the S-18 and S-28 sample (see Fig. 8a and b). However, with the N2 flow rate increases, fewer cracks are observed in the interior of the scratches for the S-38 sample. Thus, it is found that the adhesion behaviors can be altered by tuning N₂ flow rate. Viewing the failure morphology of the coatings, the most excellent fracture resistance behavior is obtained for the S-38 sample, which is contributed by its densest and finest columnar structure. In addition, the cracks in the scratch of the S-48 sample are the finest and there is no obvious large flaking in the entire scratch track, although its L_{C1} value is the lowest. Generally speaking, the fracture toughness and hardness of the coating show an inverse relationship [29]. The S-48 sample possesses the excellent toughness caused by the weakened hardness, which

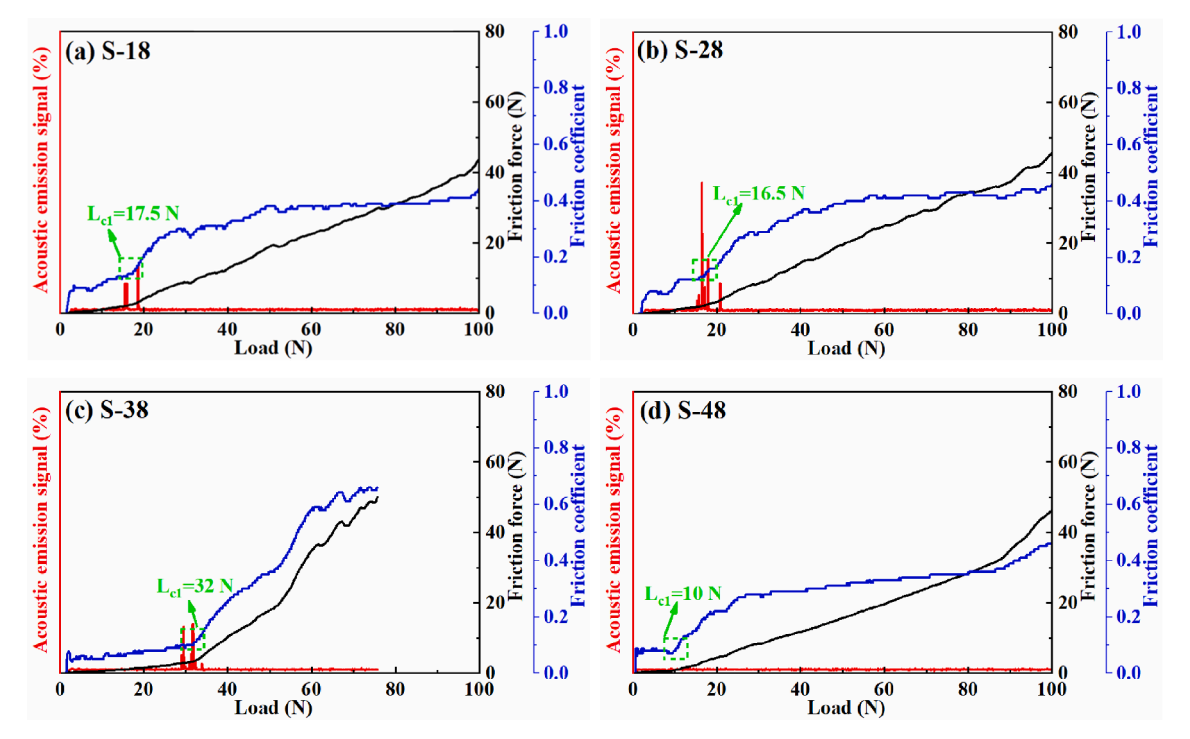


Fig. 7. Scratch tests in the (CrAlTiNbV)N_x coatings deposited at different N₂ flow rates: (a) 18 sccm; (b) 28 sccm; (c) 38 sccm and (d) 48 sccm.

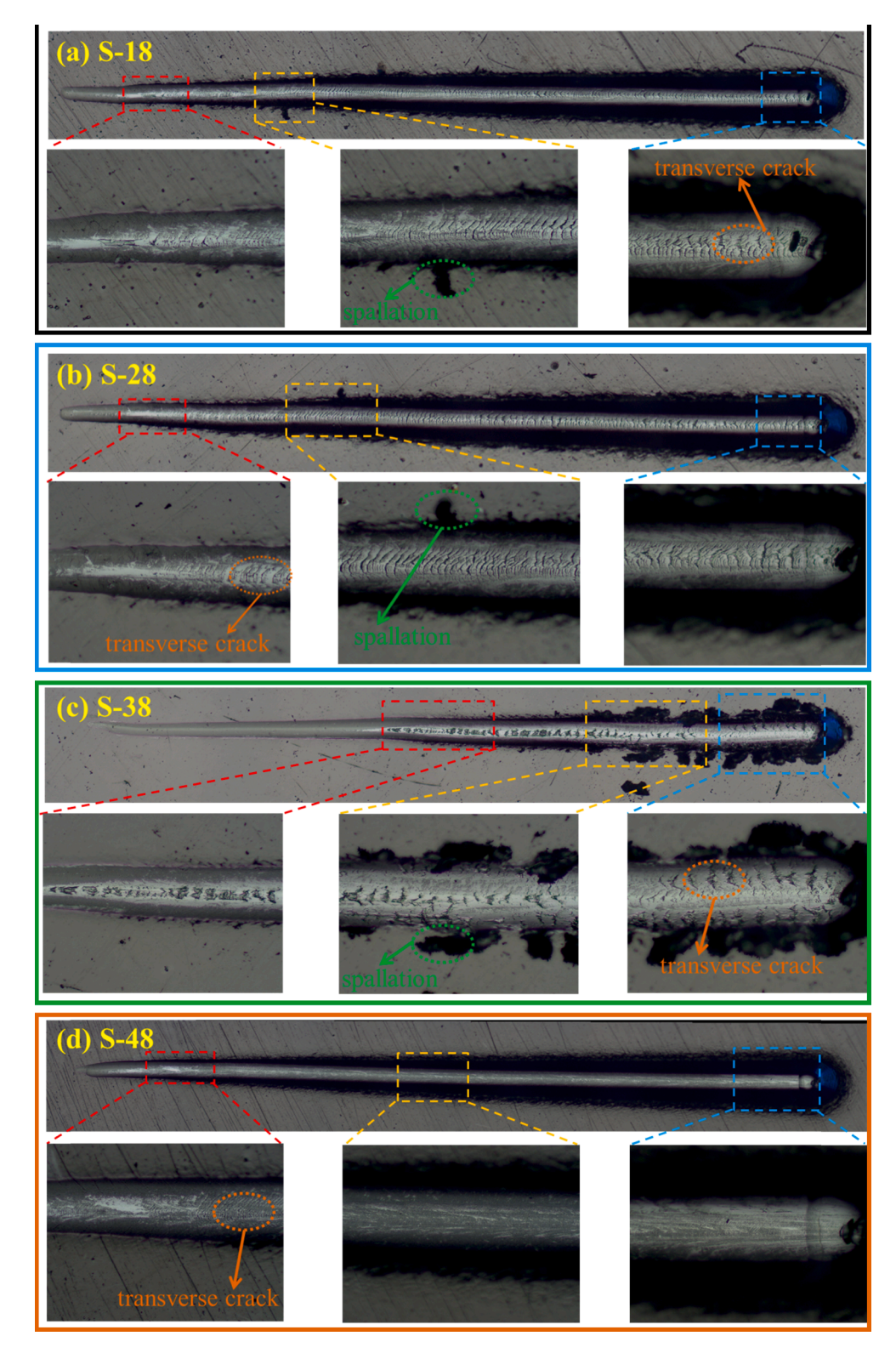


Fig. 8. Scratch images in the (CrAlTiNbV) $\!N_x$ coatings with different N_2 flow rates.

makes the coating difficult to peel off from the substrate, so as to obtain a better adhesion behavior.

Fig. 9 and Fig. 10 present the friction coefficient and wear rate of AISI 440C steel substrate and (CrAlTiNbV) N_x coatings with varying N_2 flow rates. In the atmospheric environment, the average value of friction coefficient for steel substrate in 4050# oil is near 0.12. As (CrAlTiNbV) N_x coatings are deposited, it is mentioned that the friction coefficient

varies in the range of 0.096–0.115 for all deposited coatings. The friction coefficient of (CrAlTiNbV)Nx coatings first decreases and then increases with the N2 flow rate increases. The result reveals that the S-38 sample in 4050# oil owns the steady state friction coefficient, which possesses the lowest friction coefficient (0.096). After the wear test, the lowest wear rate is $1.8\times10^{-7}\,\text{mm}^3/(\text{N}\cdot\text{m})$ for the S-38 sample in 4050# aviation oil, while the wear rate of steel substrate reaches up $5.68\times10^{-6}\,\text{mm}^3/$

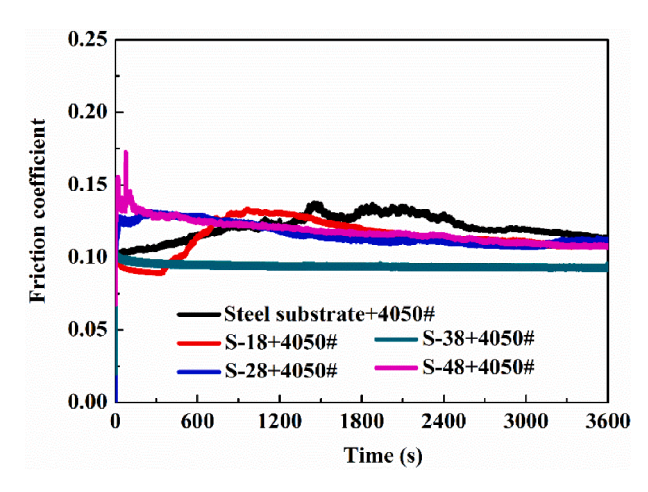


Fig. 9. Friction coefficients of AISI 440C steel and (CrAlTiNbV) N_x coatings deposited at different N_2 flow rates in 4050# aviation lubricant.

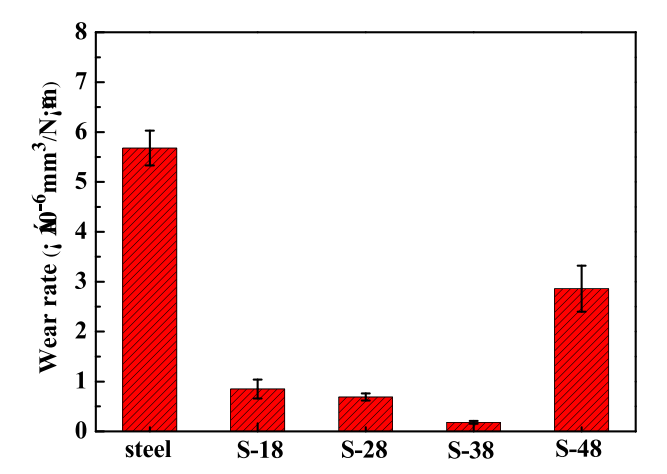


Fig. 10. Wear rates of AISI 440C steel and (CrAlTiNbV)N $_{x}$ coatings deposited at different N $_{2}$ flow rates in 4050# aviation lubricant.

(N·m). It is worth noting that the wear rate of the S-38 sample is an order of magnitude lower than that of the steel substrate. However, the wear rate apparently increases from the S-38 sample ($1.8 \times 10^{-7} \text{ mm}^3/(\text{N·m})$) to the S-48 sample ($2.86 \times 10^{-6} \text{ mm}^3/(\text{N·m})$) in 4050# aviation oil. This

demonstrates that the N_2 flow rate plays a significant role in the tribological properties of the coatings, while the optimal effect is obtained at the S-38 sample owing to its dense and compact structure.

Fig. 11 shows the wear track images of AISI 440C steel substrate and (CrAlTiNbV)N_x coatings deposited at different N₂ flow rates. The wear tracks and ribbon-like ploughing scar can be apparently observed, and the abrasion grooves are parallel to the sliding direction in all coatings, which indicate abrasive wear mechanism. It can be found that the width of wear track for the S-38 sample is the narrowest, which corresponds to the lowest wear rate. The wear tracks of the steel substrate and the S-48 sample show wider and deeper grooves in comparison to others, which is consistent with its higher wear rates. On the contrary, the wear tracks for the S-18 and S-28 sample are narrower than that of steel substrate, indicating its lower wear rates. In short, a third-body abrasive wear mechanism is dominant, and the tribo-products that fall off the wear tracks are attached to the friction pair, resulting in scratching and ploughing on these grooves. The S-38 sample is considered to be more resistant to wear, and possesses the optimal anti-wearing behavior. In summary, a dense and compact structure of the S-38 sample can contribute to a less abrasive wear, and thus the load-bearing capacity of the coatings is improved. The loose coarse columnar structure of the coatings accompanied by a defective structure, such as high void concentration, can allow the lubricant to penetrate into the coating microstructure, which makes the coating prone to corrosion. What's more serious is that the lubricant can penetrate into the transition layer, and then affect the adhesion behavior of the coatings. Besides, the excellent mechanical properties of the coatings, reflected by the resistance of plastic deformation and fracture behavior, can impact the wear rate of the coatings [30]. The corresponding synergistic lubricating mechanism is displayed in Fig. 12. The coating on the left has a loose structure and poor adhesion strength, which leads to cracks and peeling during the friction process. By adjusting the N2 flow rate, a dense, highcohesive coating on the right can be obtained. This kind of coating (such as the S-38 sample) has less cracks and peeling during the friction process, and the tribological properties are the best, which is also consistent with the results of the friction and wear experiments.

4. Conclusions

High entropy nitride $(CrAlTiNbV)N_x$ coatings are successfully fabricated via tuning N_2 flow rates by magnetron sputtering technique. The main conclusions are as follows:

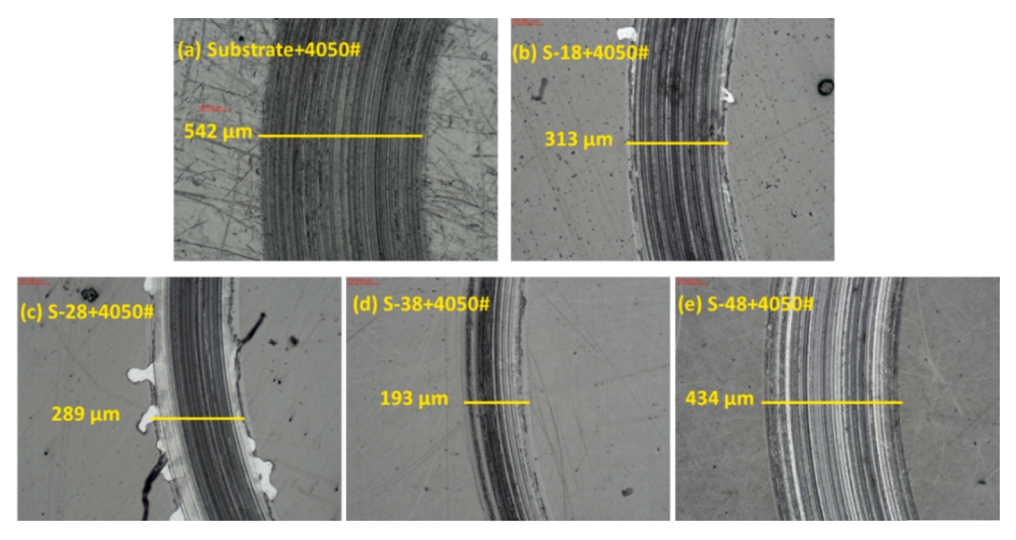


Fig. 11. Wear track images of (a) AISI 440C steel and (b-e) (CrAlTiNbV)N_x coatings deposited at different N₂ flow rates in 4050# aviation lubricant.

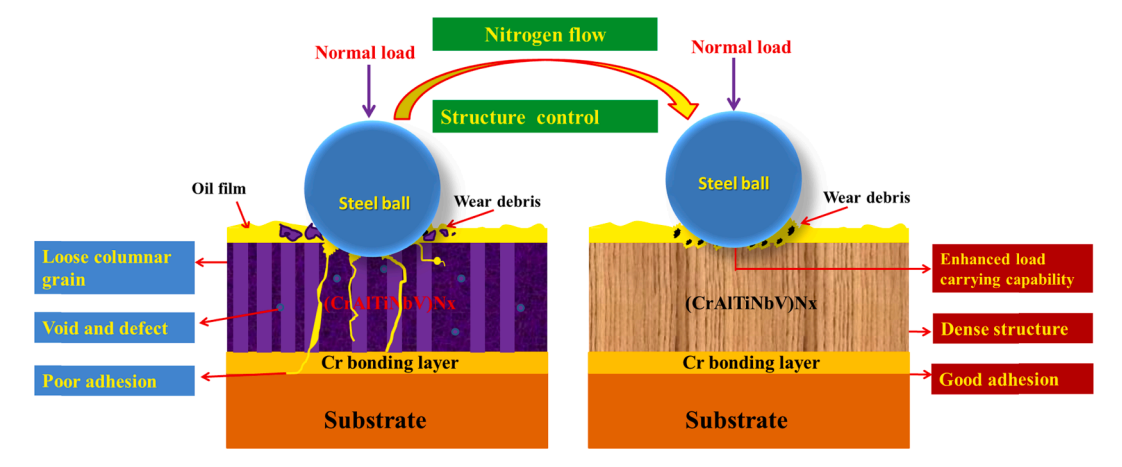


Fig. 12. Schematic diagram for revealing the synergistic lubricating mechanism of (CrAlTiNbV)N_x coatings in 4050# aviation lubricant.

- (1) As the N₂ flow rate increases, the coating microstructure presents a denser and finer columnar structure, and the S-38 sample achieves the densest and finest columnar structure, while a larger size of the columnar crystal is exhibited as the N₂ flow rate continues to increase to 48 sccm.
- (2) The (CrAlTiNbV) N_x coatings exhibit a single FCC solid solution structure, instead of multi-phase complex structures. The preferred orientation of the coating gradually changes from (111) to (200) and (220) as the N_2 flow rate increases from 18 sccm to 38 sccm, and then changes back to (111) for the S-48 sample, which can be explained in terms of thermodynamics and kinetics.
- (3) The S-38 sample possesses the optimal plastic deformation resistance and adhesion strength, which is contributed by the densest and finest columnar structure.
- (4) As the N_2 flow rate increases, the friction coefficient and wear rate of the coatings first decrease and then increase. The S-38 sample exhibits the lowest average friction coefficient (0.096) and the lowest wear rate $(1.8 \times 10^{-7} \text{ mm}^3/(\text{N·m}))$ in 4050# aviation lubricant. The densest and finest columnar structure and the excellent mechanical properties are believed to be responsible for the excellent tribological properties of the S-38 sample.
- (5) This study confirms that (CrAlTiNbV)N_x coatings can improve the wear resistance of substrate in 4050# aviation lubricant. Therefore, state of the art high entropy nitride coatings possess great promise for aviation industry applications.

CRediT authorship contribution statement

Xiaolong Lu: Conceptualization, Methodology, Investigation, Validation, Formal analysis, Writing - original draft, Visualization. Cunxiu Zhang: Investigation. Cong Wang: Investigation. Xinjian Cao: Investigation. Rui Ma: Investigation, Methodology. Xudong Sui: Resources, Writing - review & editing, Funding acquisition. Junying Hao: Resources, Writing - review & editing, Supervision, Funding acquisition. Weimin Liu: Supervision, Project administration, Funding acquisition.

Declaration of Competing Interest

The authors declare that they have no known competing financial interests or personal relationships that could have appeared to influence the work reported in this paper.

Acknowledgments

The authors gratefully acknowledge the financial support of National Natural Science Foundation of China (51835012, 51805515), the

National Key R&D Plan of China (No. 2018YFB0703803), the program of "Science & Technology International Cooperation Demonstrative Base of Metal Surface Engineering along the Silk Road (2017D01003)," and CAS "Light of West China".

References

- [1] Q.C. Chen, G.Z. Wu, D.S. Li, A. Li, L.L. Shang, Z.B. Lu, G.G. Zhang, Z.G. Wu, G. K. Tian, Understanding the unusual friction behavior of TiN films in vacuum, Tribol. Int. 137 (2019) 379–386, https://doi.org/10.1016/j.triboint.2019.05.024.
- [2] P. Tan, L.C. Fu, J. Teng, J.J. Zhu, W.L. Yang, D.Y. Li, L.P. Zhou, Effect of texture on wear resistance of tantalum nitride film, Tribol. Int. 133 (2019) 126–135, https:// doi.org/10.1016/j.triboint.2019.01.001.
- [3] A.A. Bagdasaryan, A.V. Pshyk, L.E. Coy, M. Kempinski, A.D. Pogrebnjak, V. M. Beresnev, S. Jurga, Structural and mechanical characterization of (TiZrNbHfTa) N/WN multilayered nitride coatings, Mater. Lett. 229 (2018) 364–367, https://doi.org/10.1016/j.matlet.2018.07.048.
- [4] F. Guo, K.S. Li, X.F. Huang, Z.W. Xie, F. Gong, Understanding the wear failure mechanism of TiAlSiCN nanocomposite coating at evaluated temperatures, Tribol. Int. 154 (2021) 8, https://doi.org/10.1016/j.triboint.2020.106716.
- [5] W. Li, P. Liu, P.K. Liaw, Microstructures and properties of high-entropy alloy films and coatings: a review, Mater. Res. Lett. 6 (2018) 199–229, https://doi.org/ 10.1080/21663831.2018.1434248.
- [6] E. Lewin, Multi-component and high-entropy nitride coatings-A promising field in need of a novel approach, J. Appl. Phys. 127 (2020), 160901, https://doi.org/ 10.1063/1.5144154
- [7] X.Y. Sun, X.W. Cheng, H.N. Cai, S. Ma, Z.Q. Xu, T.Y. Ali, Microstructure, mechanical and physical properties of FeCoNiAlMnW high-entropy films deposited by magnetron sputtering, Appl. Surf. Sci. 507 (2020), 145131, https://doi.org/ 10.1016/j.apsusc.2019.145131.
- [8] Q.F. Ye, K. Feng, Z.G. Li, F.G. Lu, R.F. Li, J. Huang, Y.X. Wu, Microstructure and corrosion properties of CrMnFeCoNi high entropy alloy coating, Appl. Surf. Sci. 396 (2017) 1420–1426, https://doi.org/10.1016/j.apsusc.2016.11.176.
- [9] E.J. Pickering, N.G. Jones, High-entropy alloys: a critical assessment of their founding principles and future prospects, Int. Mater. Rev. 61 (2016) 183–202, https://doi.org/10.1080/09506608.2016.1180020.
- [10] M.H. Tsai, J.W. Yeh, High-Entropy Alloys: A Critical Review, Mater. Res. Lett. 2 (2014) 107–123, https://doi.org/10.1080/21663831.2014.912690.
- [11] C.H. Lai, S.J. Lin, J.W. Yeh, S.Y. Chang, Preparation and characterization of AlCrTaTiZr multi-element nitride coatings, Surf. Coat. Technol. 201 (2006) 3275–3280, https://doi.org/10.1016/j.surfcoat.2006.06.048.
- [12] K.H. Cheng, C.H. Lai, S.J. Lin, J.W. Yeh, Structural and mechanical properties of multi-element (AlCrMoTaTiZr)N_x coatings by reactive magnetron sputtering, Thin Solid Films 519 (2011) 3185–3190, https://doi.org/10.1016/j.tsf.2010.11.034.
- [13] P.K. Huang, J.W. Yeh, Effects of substrate temperature and post-annealing on microstructure and properties of (AlCrNbSiTiV)N coatings, Thin Solid Films 518 (2009) 180–184, https://doi.org/10.1016/j.tsf.2009.06.020.
- [14] P.K. Huang, J.W. Yeh, Inhibition of grain coarsening up to 1000 degrees C in (AlCrNbSiTiV)N superhard coatings, Scr. Mater. 62 (2010) 105–108, https://doi. org/10.1016/j.scriptamat.2009.09.015.
- [15] Z.C. Chang, S.C. Liang, S. Han, Y.K. Chen, F.S. Shieu, Characteristics of TiVCrAlZr multi-element nitride films prepared by reactive sputtering, Nucl. Instrum. Methods Phys. Res. Sect. B-Beam Interact. Mater. Atoms. 268 (2010) 2504–2509, https://doi.org/10.1016/j.njmb.2010.05.039.
- [16] W.J. Shen, M.H. Tsai, Y.S. Chang, J.W. Yeh, Effects of substrate bias on the structure and mechanical properties of ($Al_{1.5}$ CrNb_{0.5}Si_{0.5}Ti)N_x coatings, Thin Solid Films 520 (2012) 6183–6188, https://doi.org/10.1016/j.tsf.2012.06.002.
- [17] P.K. Huang, J.W. Yeh, Effects of substrate bias on structure and mechanical properties of (AlCrNbSiTiV)N coatings, J. Phys. D:Appl. Phys. 42 (2009), 115401, https://doi.org/10.1088/0022-3727/42/11/115401.

- [18] Y.C. Lin, S.Y. Hsu, R.W. Song, W.L. Lo, Y.T. Lai, S.Y. Tsai, J.G. Duh, Improving the hardness of high entropy nitride (Cr_{0.35}Al_{0.25}Nb_{0.12}Si_{0.08}V_{0.20})N coatings via tuning substrate temperature and bias for anti-wear applications, Surf. Coat. Technol. 403 (2020), 126417, https://doi.org/10.1016/j.surfcoat.2020.126417.
- [19] S.C. Liang, D.C. Tsai, Z.C. Chang, H.S. Sung, Y.C. Lin, Y.J. Yeh, M.J. Deng, F. S. Shieu, Structural and mechanical properties of multi-element (TiVCrZrHf)N coatings by reactive magnetron sputtering, Appl. Surf. Sci. 258 (2011) 399–403, https://doi.org/10.1016/j.apsusc.2011.09.006.
- [20] M.H. Hsieh, M.H. Tsai, W.J. Shen, J.W. Yeh, Structure and properties of two Al-Cr-Nb-Si-Ti high-entropy nitride coatings, Surf. Coat. Technol. 221 (2013) 118–123, https://doi.org/10.1016/j.surfcoat.2013.01.036.
- [21] P.K. Huang, J.W. Yeh, Effects of nitrogen content on structure and mechanical properties of multi-element (AlCrNbSiTiV)N coating, Surf. Coat. Technol. 203 (2009) 1891–1896, https://doi.org/10.1016/j.surfcoat.2009.01.016.
- [22] S.C. Liang, Z.C. Chang, D.C. Tsai, Y.C. Lin, H.S. Sung, M.J. Deng, F.S. Shieu, Effects of substrate temperature on the structure and mechanical properties of (TiVCrZrHf) N coatings, Appl. Surf. Sci. 257 (2011) 7709–7713, https://doi.org/10.1016/j. apsusc 2011.04.014
- [23] M.H. Tsai, C.H. Lai, J.W. Yeh, J.Y. Gan, Effects of nitrogen flow ratio on the structure and properties of reactively sputtered (AlMoNbSiTaTiVZr)N_x coatings, J. Phys. D:Appl. Phys. 41 (2008), 235402, https://doi.org/10.1088/0022-3727/ 41/2/235403
- [24] D.C. Tsai, Y.L. Huang, S.R. Lin, S.C. Liang, F.S. Shieu, Effect of nitrogen flow ratios on the structure and mechanical properties of (TiVCrZry)N coatings prepared by

- reactive magnetron sputtering, Appl. Surf. Sci. 257 (2010) 1361–1367, https://doi.org/10.1016/j.apsusc.2010.08.078.
- [25] Y. Zhang, X.H. Yan, W.B. Liao, K. Zhao, Effects of nitrogen content on the structure and mechanical properties of $(Al_{0.5}CrFeNiTi_{0.25})N_x$ high-entropy films by reactive sputtering, Entropy. 20 (2018) 624, https://doi.org/10.3390/e20090624.
- [26] P.P. Cui, W. Li, P. Liu, K. Zhang, F.C. Ma, X.H. Chen, R. Feng, P.K. Liaw, Effects of nitrogen content on microstructures and mechanical properties of (AlCrTiZrHf)N high-entropy alloy nitride films, J. Alloy. Compd. 834 (2020) 6, https://doi.org/ 10.1016/j.jallcom.2020.155063.
- [27] W.L. Lo, S.Y. Hsu, Y.C. Lin, S.Y. Tsai, Y.T. Lai, J.G. Duh, Improvement of high entropy alloy nitride coatings (AlCrNbSiTiMo)N on mechanical and high temperature tribological properties by tuning substrate bias, Surf. Coat. Technol. 401 (2020), https://doi.org/10.1016/j.surfcoat.2020.126247.
- [28] K.H. Cheng, C.H. Weng, C.H. Lai, S.J. Lin, Study on adhesion and wear resistance of multi-element (AlCrTaTiZr)N coatings, Thin Solid Films 517 (2009) 4989–4993, https://doi.org/10.1016/j.tsf.2009.03.139.
- [29] X.D. Sui, G.J. Li, C.J. Jiang, K. Wang, Y.J. Zhang, J.Y. Hao, Q. Wang, Improved toughness of layered architecture TiAlN/CrN coatings for titanium high speed cutting, Ceram. Int. 44 (2018) 5629–5635, https://doi.org/10.1016/j.ceramint.2017.12.210.
- [30] X.D. Sui, J.Y. Liu, S.T. Zhang, J. Yang, J.Y. Hao, Microstructure, mechanical and tribological characterization of CrN/DLC/Cr-DLC multilayer coating with improved adhesive wear resistance, Appl. Surf. Sci. 439 (2018) 24–32, https://doi. org/10.1016/j.apsusc.2017.12.266.